Unconventional generation of optical vortex beam using axicon pair and a birefringent lens: Validation of plasmonic excitation

Jayeta Banerjee and Mina Ray

Citation: Appl. Phys. Lett. **110**, 181105 (2017); doi: 10.1063/1.4982875
View online: http://dx.doi.org/10.1063/1.4982875
View Table of Contents: http://aip.scitation.org/toc/apl/110/18
Published by the American Institute of Physics

Unconventional generation of optical vortex beam using axicon pair and a birefringent lens: Validation of plasmonic excitation

Jayeta Banerjee[a] and Mina Ray[b]
Department of Applied Optics and Photonics, University of Calcutta (Technology Campus), Acharya Prafulla Chandra Siksha Prangan, JD-2, Salt Lake, Sec-III, Kolkata 700 106, India

(Received 10 January 2017; accepted 20 April 2017; published online 1 May 2017)

We generate a nondiffracted Bessel beam using an axicon. A simple setup is presented to generate a zero order Bessel beam. Moreover, we introduce certain modifications in this optical setup for unconventional generation of an optical vortex beam using an axicon pair and a birefringent lens. An optical vortex beam with a topological charge of 1 is generated, and the corresponding spiral pattern has been demonstrated, which confirms the presence of orbital angular momentum in the optical vortex beam. Further, plasmonic excitation is validated using both zero order and first order Bessel beams. Our approach to confirm the presence of surface plasmon resonance relies on the use of a Wollaston prism. We are able to separately identify the coupling of surface plasmons with the p-polarized components via the absence of the corresponding annular beam. *Published by AIP Publishing*. [http://dx.doi.org/10.1063/1.4982875]

In recent years, the study and the generation of optical vortices (OVs) have attracted considerable research interest where a Bessel beam plays an important role. A Bessel beam is characterized by a radial wave vector (k_ρ) and an azimuthal index (l), resulting in the generation of helical wavefronts.[1] It can be generated in a number of ways: by the use of an annulus and a lens, a hologram,[2,3] a spatial light modulator,[4] or an axicon.[5]

Higher order Bessel beams have helical wavefronts and carry orbital angular momentum (OAM). They have been experimentally generated using an axicon illuminated by a Laguerre–Gaussian beam.[6] As the order of the Bessel beam increases, the diameter of the central dark ring also increases. Spin angular momentum (SAM) corresponds to polarization, whereas OAM corresponds to the azimuthal phase. SAM to OAM conversion has been discussed in Ref. 7. The generation of scalar and vectorial vortex beams by using a homogeneous anisotropic medium instead of using an inhomogeneous birefringent medium has been reported.[8] The generation of higher order OVs with topological charges of ± 1 and ± 2 have been demonstrated by O'Dwyer *et al.*[9] by cascaded conical diffraction using two biaxial crystals and recently by Zhang *et al.*[10] using cascaded acoustically driven vector mode conversion.

Special attention is paid to the second harmonic generation using uniaxial crystals as Bessel beams hold significant potential in nonlinear optics.[11] The interference pattern due to the circular polarized Gaussian beam propagating along the optic axis of the uniaxial crystal has been observed experimentally and theoretically.[12] The experimental generation of the first order Bessel beam by the interference of cosine and sine components has been performed using a Mach-Zehnder set up.[13] As reported by many researchers, conventional vortices can be generated by the Fourier transform of a Bessel beam, and the ring diameter depends on the topological charge. But the challenge requiring ring diameter to be independent of topological charge is the generation of a perfect vortex as demonstrated theoretically and verified experimentally in Ref. 14.

OV beams are often employed for the generation of surface plasmon polaritons (SPPs).[15] Surface plasmon resonance (SPR) occurs for p-polarization under the attenuated total reflection (ATR) coupler mode, satisfying phase matching conditions.[16] Parameter like reflectance-dip/transmittance-peak/phase-jump at resonance is very sensitive to change in the optical properties of the analyte in the vicinity of the metal surface and has been extensively used for nanoplasmonic sensing.[17]

Efficient coupling of the incident energy to the surface plasmon (SP) mode can be ensured by optimum choice of metal layer thickness[18] in a conventional Kretschmann structure. The phase detection based SPR interferometric technique provides higher resolution. In this context, phase response curves for different oxygenated hemoglobins have been analyzed, and the minimum detectable refractive index (RI) of order of 10^{-8} RIU has been theoretically achieved by us. We have reported SPR modulated radially sheared interference imaging using a birefringent lens (BL).[19,20] The main components used in our approach were BL and Wollaston prism (WP) to generate plasmonic moiré surfaces without going into the complicated fabrication process of sub-wavelength grating generally employed for the generation of such nano-patterns.[21]

Advantages of Bessel beams in applications such as microscopy and imaging are equally applicable to SPR excitation and related applications. First experimental surface plasmon polariton excitation using a zero order Bessel beam has been reported by Kano *et al.*[22] A detailed theory of evanescent Bessel beams via surface plasmon excitation with a tightly focused radially polarized beam is presented in Ref. 23. The dark ring confirming SPR excitation and decaying nature of the evanescent Bessel beam have been reported by collection mode near-field scanning optical microscopy.[24] Kurilkina *et al.*[25] have analyzed different types of surface

[a]E-mail: j.banerjee87@yahoo.com
[b]Author to whom correspondence should be addressed. Electronic mail: mraphy@caluniv.ac.in. Tel.: 91 33 23352411. Fax: 91 33 23522411.

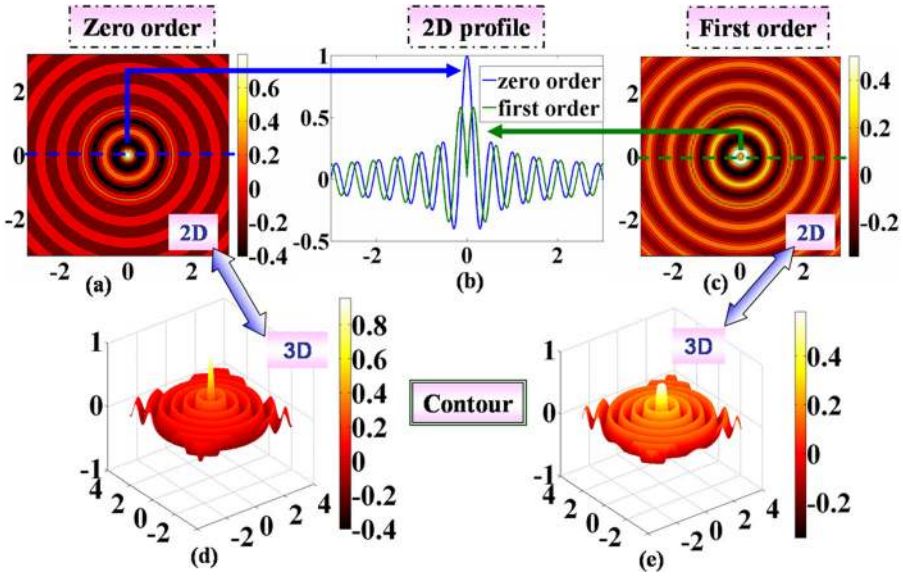

FIG. 1. Simulated (a) zero and (c) first order Bessel beams. The corresponding intensity curves of (a) and (c) are shown in (b). Contour plots of (a) and (c) are shown in (d) and (e), respectively.

plasmon polariton based symmetric and asymmetric "dielectric-metal-dielectric" structures.

In this letter, we propose and experimentally demonstrate an unconventional approach to generate a higher order vortex through the combination of an axicon pair and a BL. The cylindrical beam carrying OAM is also experimentally demonstrated. To further validate our proposed approach in plasmonic modulation, a WP is adopted to decompose the resultant beam into two orthogonally polarized beams. The proposed method opens an unconventional window to generate OVs using axicon-BL combination.

Mathematical description for a cylindrical vector beam is well established.[26] For the benefit of general readers, it is necessary to include generalized formulation on which our simulations are based. The electric field of the Bessel beam in the vicinity of the focus can be calculated with the Richards–Wolf vectorial diffraction theory.[27] The amplitude of the electric field follows a Bessel function in the radial coordinate, modulated by an azimuthal phase variation $E(\rho, \phi, z) \propto J_l(k_\rho \rho)\ \exp(ik_z z) \exp(il\phi)$, where J_l is the lth order Bessel function, k_ρ and k_z are the radial and longitudinal wavevectors, where $k = \sqrt{k_\rho^2 + k_z^2} = 2\pi/\lambda$ (λ is the wavelength of the electromagnetic radiation), and ρ, ϕ, and z correspond to the radial, azimuthal, and longitudinal components, respectively. Here, k_ρ determines the spacing of the Bessel beam rings, and the azimuthal index, l, determines both the order of the Bessel beam and the azimuthal phase variation.[1,28]

Theoretically computed zero-order and first-order Bessel functions along with intensity distributions are shown in Figure 1. The zero-order beam has a bright central maximum as shown in Fig. 1(a), whereas the first-order beam has a dark centre shown in Fig. 1(c). The 2D profile (Fig. 1(b)) and 3D contour profiles (Figs. 1(d) and 1(e)) are computed for zero and first order Bessel beams, respectively.

Fig. 2 shows the schematic of the setup for the generation of a zero order Bessel beam. The expanded collimated Gaussian beam (He-Ne laser, $\lambda = 632.8$ nm) is passed through a polarizer whose transmission axis is at 45° followed by a quarter wave plate (QWP) whose fast axis is vertical, thus generating a circularly polarized beam. The axicon-generated Bessel beam is focused on to the hypotenuse surface of an Aluminium(Al)-coated BK7 glass prism using a zoom lens. The reflected divergent beam is focused onto the WP with the help of a lens. Two mutually orthogonal beams emerging from the WP are passed through an analyzer and a lens and finally captured on a CCD. We have used the WP with its axis adjusted in order to laterally separate the p- and s-polarization. Then transmission axis of the analyzer is matched with the transmission axis of the WP. The purpose of using the analyzer is just to reduce the intensity of the pattern.

The electric field of the generalized plane cylindrical beam can be written as[26]

$$\bar{E}(\rho, \varphi, z) = E_\rho \hat{e}_\rho + E_z \hat{e}_z + E_\varphi \hat{e}_\varphi. \tag{1}$$

The field components in the radial, azimuthal, and propagation directions are E_ρ, E_φ, E_z, respectively, which are given as[29]

$$\begin{aligned} E_\rho(\rho, \varphi, z) &= A \int_0^\alpha \cos^{1/2}\theta\ \sin 2\theta J_1(k\rho \sin\theta)\, e^{ikz\cos\theta} d\theta \\ &= 2A \int_0^\alpha \cos^{1/2}\theta\ \sin\theta\ \cos\theta J_1(k\rho \sin\theta)\ e^{ikz\cos\theta} d\theta, \end{aligned} \tag{2}$$

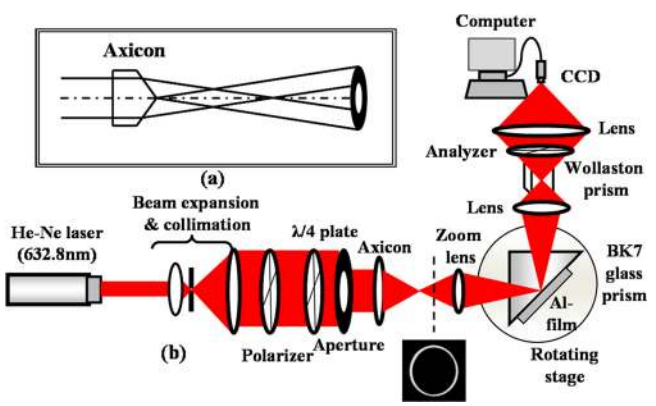

FIG. 2. Schematic diagram for the generation of a Bessel beam using an axicon illuminated with a Gaussian beam. (b) Experimental setup for the generation of a zero-order Bessel beam for plasmonic modulation.

$$E_\varphi(\rho,\varphi,z) = 2A\int_0^\alpha \cos^{1/2}\theta\,\sin\theta J_1(k\rho\sin\theta)\,e^{ikz\cos\theta}d\theta, \quad (3)$$

$$E_z(\rho,\varphi,z) = 2iA\int_0^\alpha \cos^{1/2}\theta\sin^2\theta J_0(k\rho\sin\theta)\,e^{ikz\cos\theta}d\theta, \quad (4)$$

where $\alpha = \sin^{-1}(NA)$ of the objective lens. The pupil apodization function is considered to be unity. In our case, the field distribution is in the ρ-z plane. Therefore,

$$\bar{E} = E_\rho\hat{e}_\rho + E_z\hat{e}_z. \quad (5)$$

The phase matching condition for SPR occurrence is given by

$$\sqrt{\varepsilon_{pr}}\frac{\omega}{c}\sin\theta = \frac{\omega}{c}\sqrt{\frac{\varepsilon_1\varepsilon_2}{\varepsilon_1+\varepsilon_2}}, \quad (6)$$

where ε_{pr}, ε_1, and ε_2 are the dielectric permittivities of the prism, metal, and dielectric layer, respectively, for the three layer SPR configuration and θ is the incident angle in the prism.

In order to incorporate the SPR effect in the beam, the transmission coefficient of the p-polarization at the incident angle of θ, i.e., $t_p(\theta)$, is to be accommodated within the integral.[22]

Then,

$$E_\rho(\rho,\varphi,z) = 2A\int_0^\alpha \cos^{1/2}\theta\,\sin\theta\,\cos\theta\,t_p(\theta) \times J_1(k\rho\sin\theta)\,e^{ikz\cos\theta}d\theta \quad (7)$$

and

$$E_z(\rho,\varphi,z) = 2iA\int_0^\alpha \cos^{1/2}\theta\sin^2\theta\,t_p(\theta)\,J_0(k\rho\sin\theta)\,e^{ikz\cos\theta}d\theta. \quad (8)$$

The change in the ring pattern due to SPR excitation as shown in Fig. 3 was observed using the setup described in Fig. 2. It is seen that two annular beams are formed after passing through the WP corresponding to two orthogonal polarization components. For the beam reflected from the uncoated prism satisfying the resonance angle, annular beams are found to remain unaltered, whereas for a 38 nm Al-coated BK7 prism, one annular ring disappears under the same conditions as shown in Fig. 3(a).

In our case, the incident circular polarized beam comprises of equal amplitude p- and s-polarization components. After passing through the axicon, the generated Bessel beam contains both radial polarized (RP) and azimuthal polarized (AP) components. Comparing p- and s-polarization with the RP and AP beams, both p- and RP beams are TM polarized, while s- and AP beams are TE polarized. When a beam (containing both orthogonal polarized components) is used to excite SP in a common optical path, only the reflected light

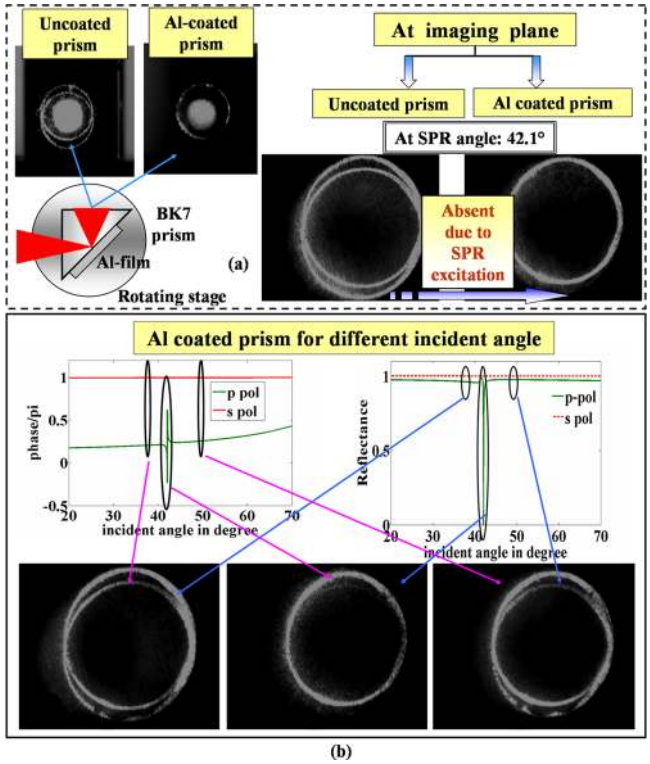

FIG. 3. (a) Experimental images for uncoated and Al coated BK7 glass prisms for the SPR angle at (left) the plane of the prism from where the beam is emerging and (right) actual imaging plane. (b) Experimental images for the Al coated BK7 glass prism for three different incident angles.

due to the p-polarized component carries the information of SP excitation. The Bessel beam is advantageous compared to the conventional circular polarized beam due to certain unique properties such as smaller focus spot and higher coupling efficiency. The resonance parameters of the three-layer Kretschmann configuration can be calculated using Fresnel equations and the characteristic transfer matrix (CTM) method.[30] Different glass prisms can be used depending upon the working wavelength. The higher index substrate and higher wavelength provides higher field enhancement.[31] Here, the reflectance and phase response have been simulated for a wavelength of 632.8 nm as shown in Fig. 3(b). Three annular ring patterns have been captured for three different incident angles, which are indicated in the reflectance and phase response plots. The middle pattern corresponds to the SPR angle where the p-polarized annular ring is found to be absent. In all the three cases, the annular ring that corresponds to s-polarization remains almost the same.

Next, we present an unconventional generation of the OAM-carrying OV beam. Our approach is to convert impinging circularly polarized light to an OAM state by using an axicon pair and a BL as shown in the modified set-up in Fig. 4. The actual snapshot is shown in Fig. 4(a), and the corresponding schematic diagram is shown in Fig. 4(b). The generation of a dual annular beam is shown in Fig. 4(c). We can notice from this figure that a dual annular beam consists of two cylindrical beams with different angular spreads. The BL with an uniaxial medium has been used for introducing the phase delay between the ordinary (o-) and extraordinary (e-) waves. As the dual annular beam is theta dependent, for each value of theta, the refractive index (RI) of the e-wave changes

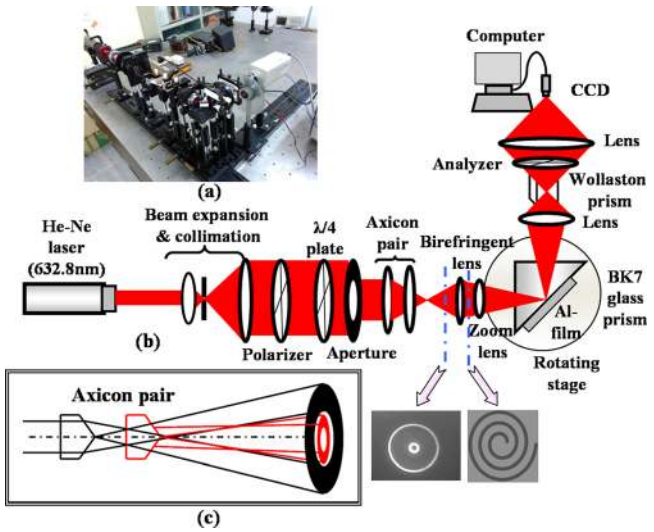

FIG. 4. (a) Actual snapshot of the experimental setup, (b) modified schematic diagram of the experimental setup for the generation of an optical vortex beam, and (c) ray diagram of dual annular beam formation using an axicon pair.

with the corresponding change in birefringence, and this is where the introduction of the azimuthal phase comes into play.

Experimental generation of the dual annular beam by using a pair of identical axicons is shown in Fig. 5(a). The spiral fringe pattern observed with the help of an analyzer after the BL confirms the presence of OAM in the OV beam. In fact, this is only possible due to the BL, which can be looked upon as a "mode converter" as the input dual annular Bessel beam is transformed into a higher order Bessel beam carrying OAM. It is quite well-known that the number of spiral patterns represents the order or the topological charge of the vortex, and its direction of rotation decides its sign. Here, we have generated the topological charge of 1 as confirmed by one spiral pattern (Fig. 5(b)). The theoretically simulated counterpart of the spiral pattern is shown in Fig. 5(c).

Next, we proceed to realize SPR modulation using the generated OV beam. A pair of dual annular beams having orthogonal polarizations is generated using a WP as shown in Fig. 6(a) for an uncoated BK7 glass prism. Here, two rings of different radii are not because of different topological charges. Both correspond to the same topological charge of order 1. The vortex beam of two rings is different from conventional generation of the vortex beam as it is generated by an axicon pair. Figure 4(c) shows how two rings of different radii are generated. The selection of individual orthogonal polarization by using an analyzer is illustrated in Fig. 6(c).

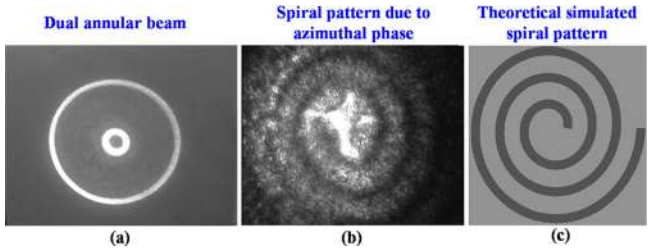

FIG. 5. (a) Dual annular pattern captured after axicon pair, (b) spiral pattern formation after the BL, and (c) spiral pattern by theoretical simulation.

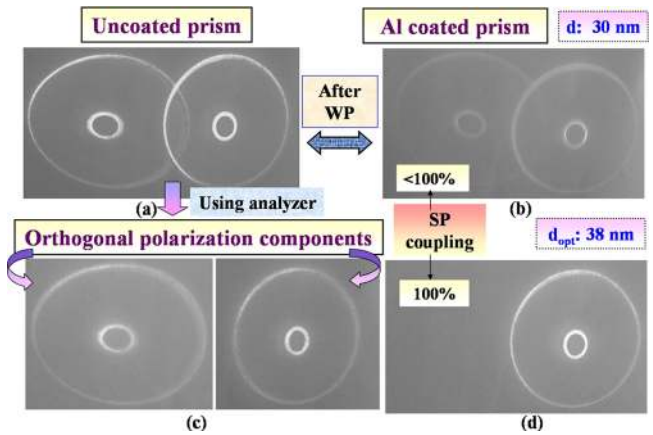

FIG. 6. Dual annular pattern captured beyond the WP at the SPR angle for (a) the uncoated prism and (b) the 30 nm Al coated prism. (c) Selection of polarization components using an analyzer for the uncoated prism. (d) Dual annular pattern for the 38 nm Al coated prism under the same SPR angle.

Moreover, to emphasize the importance of the optimum metal thickness, a 30 nm Al-coated prism (less than optimum thickness) has been used, and we have noticed that orthogonal polarization related information is present but one component is less intense than the other due to lower coupling as shown in Fig. 6(b). On the other hand, one annular beam completely disappears for the 38 nm Al-coated BK7 glass prism (Fig. 6(d)), which reveals 100% coupling of the p-polarized component to the SPP mode.

In conclusion, we proposed and experimentally demonstrated an unconventional approach to generate a vortex beam. The uniqueness of the proposed method lies in the combined contribution of the axicon pair and BL and the superposition of two orthogonal polarized light beams. The polarization distribution gets modulated due to SP excitation. As our work provides an alternate method to generate an OV beam, it opens a different field of research to be explored for future practical applications in the field of nanophotonics. The axicon provides the most efficient method of realizing diffraction-less beams. It is already reported that the diameter of the central spot of the Bessel beam is narrower than the first dark ring of the Airy pattern.[30] Thus, it provides better resolution in imaging applications. The use of an axicon proves to be advantageous in applications involving scanning.[32] Non-contact surface profilometry using SPR modulated moiré interferometry has already been proposed and reported by us.[33] In future, Bessel beams can be used instead of Gaussian beams in such an application with the added advantages offered by the present technique.

Jayeta Banerjee would like to acknowledge the Department of Science and Technology, Government of India, for financial support (Ref. No. SR/WOS-A/PM-1015/2015 dated 11/07/2016) under the Women Scientist Scheme to carry out this work. We thank Professor A. Basuray, Professor S. K. Sarkar, and Dr. M. Bera for their needful discussions during the course of this work.

[1]A. Dudley, M. Lavery, M. Padgett, and A. Forbes, Opt. Photonics News **24**(6), 22 (2013).
[2]M. Fortin, M. Piché, and E. F. Borra, Opt. Express **12**, 5887 (2004).
[3]M. R. Lapointe, Opt. Laser Technol. **24**, 315 (1992).

[4]A. Trichili, T. Mhlanga, Y. Ismail, F. S. Roux, M. McLaren, M. Zghal, and A. Forbes, Opt. Express **22**, 17553 (2014).
[5]M. de Angelisa, L. Cacciapuoti, G. Pierattini, and G. M. Tino, Opt. Laser. Eng. **39**, 283 (2003).
[6]J. Arlt and K. Dholakia, Opt. Commun. **177**, 297 (2000).
[7]T. A. Fadeyeva, V. G. Shvedov, Y. V. Izdebskaya, A. V. Volyar, E. Brasselet, D. N. Neshev, A. S. Desyatnikov, W. Krolikowski, and Y. S. Kivshar, Opt. Express **18**, 10848 (2010).
[8]C. Loussert and E. Brasselet, Opt. Lett. **35**, 7 (2010).
[9]D. P. O'Dwyer, C. F. Phelan, Y. P. Rakovich, P. R. Eastham, J. G. Lunney, and J. F. Donegan, Opt. Express **19**, 2580 (2011).
[10]W. Zhang, L. Huang, K. Wei, P. Li, B. Jiang, D. Mao, F. Gao, T. Mei, G. Zhang, and J. Zhao, Opt. Lett. **41**(21), 5082 (2016).
[11]V. N. Belyi, N. A. Khilo, N. S. Kazak, and A. A. Ryzhevich, Opt. Eng. **50**, 059001 (2011).
[12]A. Ciattoni, G. Cincotti, and C. Palma, J. Opt. Soc. Am. A **20**, 163 (2003).
[13]C. López-Mariscal, J. C. Gutiérrez-Vega, and S. Chávez-Cerda, Appl. Opt. **43**, 5060 (2004).
[14]P. Vaity and L. Rusch, Opt. Lett. **40**, 597 (2015).
[15]P. S. Tan, X.-C. Yuan, J. Lin, Q. Wang, T. Mei, R. E. Burge, and G. G. Mu, Appl. Phys. Lett. **92**, 111108 (2008).
[16]E. Kretschmann and H. Raether, Z. Naturforsch. **23A**, 2135 (1968).
[17]J. Homola, Chem. Rev. **108**, 462 (2008).
[18]M. Bera, J. Banerjee, and M. Ray, J. Mod. Opt. **61**, 182 (2014).
[19]M. Bera, J. Banerjee, and M. Ray, Appl. Phys. Lett. **104**, 251104 (2014).
[20]M. Bera, J. Banerjee, and M. Ray, J. Opt. Soc. Am. B **32**, 961 (2015).
[21]M. Bera, J. Banerjee, and M. Ray, Opt. Lett. **40**, 1857 (2015).
[22]H. Kano, D. Nomura, and H. Shibuya, Appl. Opt. **43**, 2409 (2004).
[23]Q. Zhan, Opt. Lett. **31**, 1726 (2006).
[24]W. Chen and Q. Zhan, Opt. Lett. **34**, 722 (2009).
[25]S. N. Kurilkina, V. N. Belyi, and N. S. Kazak, Int. J. Opt. **2013**, 253692 (2013).
[26]Q. Zhan, Adv. Opt. Photonics **1**, 1 (2009).
[27]B. Richards and E. Wolfs, Proc. R. Soc. London, Ser. A **253**, 358 (1959).
[28]D. Mcgloin and K. Dholakia, Contemp. Phys. **46**, 15 (2005).
[29]K. S. Youngworth and T. G. Brown, Opt. Express **7**, 77 (2000).
[30]M. Born and E. Wolf, *Principles of Optics* (Pergamon Press, New York (1989), p. 416.
[31]J. Banerjee, M. Bera, and M. Ray, J. Appl. Phys. **117**, 113102 (2015).
[32]R. Arimoto, C. Saloma, T. Tanaka, and S. Kawata, Appl. Opt. **31**, 6653 (1992).
[33]J. Banerjee, M. Bera, and M. Ray, J. Opt. Soc. Am. B **33**, 1462 (2016).